REPORT DOCUMENTATION PAGE

Form Approved OMB No. 074-0188

1. AGENCY USE ONLY (Leave blank)	2. REPORT DATE	3. REPORT TYPE AND DATES COVERED
	1996	Scientific report presented 28 January - 2 February 1996

4. TITLE AND SUBTITLE

Dispersion Model Development for Open Burn/Open Detonation Sources

5. FUNDING NUMBERS

N/A

6. AUTHOR(S)

J.C. Weil, B. Templeman, R. Banta, R. Weber, & W. Mitchell

7. PERFORMING ORGANIZATION NAME(S) AND ADDRESS(ES)

Cooperative Institute for Research in Environmental Sciences
University of Colorado
Boulder, CO

Environmental Technology Laboratory
Environmental Research Laboratories
Boulder, CO

National Exposure Research Laboratory
EPA
Research Triangle Park, NC

8. PERFORMING ORGANIZATION REPORT NUMBER

N/A

9. SPONSORING / MONITORING AGENCY NAME(S) AND ADDRESS(ES)

SERDP
901 North Stuart St. Suite 303
Arlington, VA 22203

10. SPONSORING / MONITORING AGENCY REPORT NUMBER

N/A

11. SUPPLEMENTARY NOTES

Paper presented at the Ninth Joint Conference on the Application of Air Pollution Meteorology with the Air and Waste Management Association, American Meteorological Society, Atlanta, GA, 28 January - 2 February 1996. This work was supported in part by SERDP.

12a. DISTRIBUTION / AVAILABILITY STATEMENT

Approved for public release: distribution is unlimited

12b. DISTRIBUTION CODE

A

13. ABSTRACT ***(Maximum 200 Words)***

The disposal of obsolete munitions, propellants, and manufacturing wastes is conducted at DoD and DOE facilities. The most common disposal method is open burning and open detonation of the material, which occurs in an earthen pit or bermed area. At present, the material destroyed in a single detonation typically ranges from 100 to 5000 lbs., whereas the quantity treated in a burn can be somewhat larger and last from minutes to an hour. OB/OD activities are restricted to daytime during unstable or near-neutral atmospheric stability.

14. SUBJECT TERMS

SERDP, Open burning, Open detonation, Dispersion

15. NUMBER OF PAGES

7

16. PRICE CODE N/A

17. SECURITY CLASSIFICATION OF REPORT	18. SECURITY CLASSIFICATION OF THIS PAGE	19. SECURITY CLASSIFICATION OF ABSTRACT	20. LIMITATION OF ABSTRACT
unclass.	unclass.	unclass.	UL

NSN 7540-01-280-5500

Standard Form 298 (Rev. 2-89)
Prescribed by ANSI Std. Z39-18
298-102

DISPERSION MODEL DEVELOPMENT FOR OPEN BURN/OPEN DETONATION SOURCES

by

J. C. Weil and B. Templeman
Cooperative Institute for Research in Environmental Sciences
University of Colorado
Boulder, Colorado

R. Banta and R. Weber
Environmental Technology Laboratory
Environmental Research Laboratories
Boulder, Colorado

W. Mitchell
National Exposure Research Laboratory
Environmental Protection Agency
Research Triangle Park, North Carolina

Ninth Joint Conference on the Applications of Air Pollution Meteorology
with the Air and Waste Management Association

American Meteorological Society

January 28 - February 2, 1996
Atlanta, Georgia

For presentation at the American Meteorological Society
9th Joint Conference on the Applications of Air Pollution
Meteorology with the AWMA, Atlanta, Georgia Jan. 28 - Feb. 2, 1996

12.5 DISPERSION MODEL DEVELOPMENT FOR OPEN BURN/OPEN DETONATION SOURCES

J.C. Weil* and B. Templeman

CIRES, University of Colorado
Boulder, Colorado

R. Banta and R. Weber

NOAA-ETL, Environmental Research Laboratories
Boulder, Colorado

W. Mitchell

AREAL, Environmental Protection Agency
Research Traingle Park, North Carolina

1. INTRODUCTION

The disposal of obsolete munitions, propellants, and manufacturing wastes is conducted at Department of Defense (DOD) and Department of Energy (DOE) facilities. The most common disposal method is open burning (OB) and open detonation (OD) of the material, which occurs in an earthen pit or bermed area. At present, the material destroyed in a single detonation typically ranges from 100 to 5000 lbs, whereas the quantity treated in a burn can be somewhat larger and last from minutes to an hour. OB/OD activities are restricted to daytime during unstable or near-neutral atmospheric stability.

OB/OD operations generate air pollutants and require predictions of pollutant concentrations. The pollutants include SO_2, NO_x, particulates, volatile organic compounds and toxic materials such as metals, semivolatile organics, etc. (Andrulis, 1992). For large detonations ($1 - 3 \times 10^4$ lbs), natural dust entrained by the blast is an additional contaminant. Emissions from OB/OD sources have the following unique features: 1) "instantaneous" or short-duration releases of buoyant material, 2) a wide variability in the initial cloud size, shape, and height, and 3) ambient exposure times from clouds that are much less than the typical averaging times ($\sim$ 1 hr) of air quality standards.

Dispersion models are used to estimate pollutant concentrations given the source and meteorological conditions. However, there is currently no recommended EPA dispersion model to address OB/OD sources. The most widely-used approach is INPUFF (Petersen, 1986), a Gaussian puff model, but this has several limitations as discussed below. Due to the contraints of existing models, a model development program was initiated under the DOD/DOE Strategic Environmental Research and Development Program.

In Section 2, we give an overview of the model design which is divided into "simple" and "research" components. Sections 3 and 4 describe the simple component which includes Gaussian puff and analytic plume models. This development program is in progress and is currently limited to the unstable planetary boundary layer (PBL).

2. MODEL DESIGN CONSIDERATIONS

2.1 *Background*

The development of an OB/OD dispersion model has considered: 1) the limitations of existing models, 2) current knowledge of turbulence and dispersion in the PBL, and 3) a mobile meteorological platform under development.

Limitations of existing models. INPUFF has been used to model OB/OD sources and can handle dispersion from individual puffs or clouds or from a sequence of puffs in a short-duration release. Although the Gaussian puff approach is suitable for OB/OD sources, INPUFF has the following limitations: 1) It adopts dispersion parameters (σ_y, σ_z) from the Pasquill-Gifford (PG) curves or from Irwin's (1983) scheme. 2) It includes Briggs' (1971) plume rise expressions which apply to continuous releases rather than to instantaneous sources (puffs, clouds) and does not address thermal penetration of elevated inversions capping the PBL. 3) It assumes Gaussian velocity statistics for the turbu-

* Also visiting scientist, National Center for Atmospheric Research, Boulder, CO

Corresponding author address: J.C. Weil, NCAR, P.O. Box 3000, Boulder, CO 80307

lence, whereas the vertical velocity statistics in the unstable PBL are positively skewed (Wyngaard, 1988). The skewness should be included for vertical dispersion.

For OB/OD sources, the PG curves are deficient in that they: 1) are based on dispersion from a ground-level source and short downwind distances (< 1 km), and 2) are selected using surface meteorology, which does not account for the PBL's vertical structure. For large detonations, source buoyancy can carry emissions to several 100 m or the PBL top; one must then deal with dispersion over the entire PBL.

PBL turbulence. Dispersion in the PBL depends on the turbulence length and velocity scales which differ for the unstable or convective boundary layer (CBL) and the stable boundary layer (SBL). For the CBL, the length and velocity scales are the CBL depth h and the convective velocity scale w_*. Typical values of w_* and h at midday over land are 1 - 2 m/s and 1 - 2 km. Within the "mixed layer" ($0.1h \leq z < h$), the mean wind speed and turbulence components—longitudinal σ_u, lateral σ_v, and vertical σ_w—vary little with height z; in strong convection, $\sigma_u, \sigma_v, \sigma_w \simeq 0.6w_*$.

For the SBL, the turbulence is much weaker with eddy sizes proportional to z near the surface and typically $\sim$ 10s of meters or less in the upper part of the SBL. Models and observations show that the velocity scale is the friction velocity u_* (Wyngaard, 1988), which is typically $\sim$ 0.1 m/s in strong stable stratification.

Knowledge of the PBL turbulence structure has been included in models for applications (see Venkatram and Wyngaard, 1988).

Mobile meteorological platform. A mobile meteorological platform is being developed at NOAA-ETL to obtain the PBL variables necessary for modeling since many DOD facilities are in remote locations. The platform design includes: 1) a radar wind profiler for obtaining the three wind components up to $\sim$ 3 km, 2) a radio acoustic sounding system (RASS) for temperature measurements, 3) a mini-SODAR for measuring winds and σ_w to a height of $\sim$ 200 m, 4) a mini-lidar system for obtaining the PBL depth h, and 5) a portable meteorological station for measuring near-surface winds, temperature, turbulence, and heat flux. The dispersion model is being designed for efficient use of these measurements.

2.2 *Overall Model Design*

A model hierarchy is planned including: 1) a simple computational framework for routine problems, and 2) a more detailed or research model for nonroutine problems. In the simple approach, a Gaussian puff model is adopted for instantaneous sources and puff, integrated-puff, and plume models for short-duration releases. For the research framework, a Lagrangian particle and/or puff approach is planned. Both frameworks will be considered for "onsite" use in a real-time operational mode using data from the mobile meteorological platform, i.e., for day-to-day decisions on OB/OD operations. The puff and plume models would be used for climatological analyses needed in risk assessments.

In modeling, the important aspects to address are: 1) all source-related features including the instantaneous or short-duration nature of the release, buoyancy-induced rise and dispersion, and cloud or plume penetration of elevated inversions, 2) relative and absolute dispersion expressions that explicitly include PBL turbulence variables, 3) meteorological variables including their vertical profiles from the mobile platform, and 4) a treatment for puff and plume dispersion about complex terrain.

The following models address points 1 and 2 above and must be expanded to include points 3 and 4. Further development also will address: 1) a more complete description of initial source effects (detonation cloud size and height) and inversion penetration, 2) a more complete PBL turbulence parameterization, 3) averaging time effects on concentration, 4) the entrained dust source term, and 5) deposition of gases and particles.

3. INSTANTANEOUS SOURCES

3.1 *Dispersion Model*

Concentration. For instantaneous sources or detonations, a Gaussian puff model is adopted for the short-term mean concentration (C) field:

$$C = \frac{Q}{(2\pi)^{3/2}\sigma_{rx}\sigma_{ry}\sigma_{rz}} \times \exp\left[-\frac{(x-Ut)^2}{2\sigma_{rx}^2} - \frac{y^2}{2\sigma_{ry}^2} - \frac{(z-h_e)^2}{2\sigma_{rz}^2}\right], \quad (1)$$

where Q is the pollutant mass released, U is the mean wind speed, t is the travel time, h_e is the effective puff height, and σ_{rx}, σ_{ry}, and σ_{rz} are the puff standard deviations or relative dispersion in the x, y, and z directions, respectively. Here, $h_e = h_s + \Delta h$ where h_s is the source height and Δh is the cloud rise due to buoyancy; x and y are the distances in the mean wind and crosswind directions.

Currently, we are considering two approaches for estimating the peak ground-level concentration (GLC) at a given x: 1) the peak concentration C_c in the elevated buoyant puff, and 2) a peak found from a probability distribution of concentration at a downwind receptor. The C_c is the puff centroid

concentration given by $C_c = Q/[(2\pi)^{3/2}\sigma_{rx}\sigma_{ry}\sigma_{rz}]$, where the relative dispersion parameters are generally different in the three directions. In the following, we assume $\sigma_{rx} = \sigma_{ry} = \sigma_{rz} = \sigma_r$. If C_c is used as an estimate of the peak concentration, an estimate must be made of the probability of it being brought to the surface; one possible method is given by Weil et al. (1995).

In the second approach, we require a functional form for the concentration probability distribution (e.g., a gamma distribution; Deardorff and Willis, 1988) and estimates of C and the root-mean-square concentration fluctuation σ_c due to an ensemble of meandering puffs. The probability distribution and the σ_c model remain to be selected. The C field including puff meandering is given by Eq. (1), but with $\sigma_{rx}, \sigma_{ry}, \sigma_{rz}$ replaced by the absolute dispersion parameters—$\sigma_x, \sigma_y, \sigma_z$. A Gaussian distribution for C is applicable to the SBL where the probability density function (p.d.f.) of the vertical velocity w is Gaussian. However, for the CBL, a skewed w p.d.f. is more consistent with laboratory and field data. A skewed p.d.f. is adopted here and is parameterized by the superposition of two Gaussian distributions (Weil, 1988).

The C field due to an ensemble of meandering puffs is derived from p_w following the same approach as applied to continuous plumes (Weil, 1988). The resulting expression for C is

$$C = \frac{Q}{(2\pi)^{3/2}\sigma_x\sigma_y} \exp\left(-\frac{(x-Ut)^2}{2\sigma_x^2} - \frac{y^2}{2\sigma_y^2}\right) \times \sum_{j=1}^{2} \frac{\lambda_j}{\sigma_{zj}} \exp\left(-\frac{(z-h_e-\overline{z_j})^2}{2\sigma_{zj}^2}\right) , \quad (2)$$

where $\sigma_{zj} = \sigma_j x/U$ and $\overline{z_j} = \overline{w_j}x/U$ with $j = 1, 2$. The λ_j, σ_j, and $\overline{w_j}$ $(j = 1, 2)$ are the weight, mean velocity, and standard deviation of each Gaussian p.d.f. comprising p_w. Equation (2) applies for short distances such that the plume interaction with the ground or elevated inversion is weak. The complete expression for C includes multiple cloud reflections at the ground and PBL top.

The time-averaged concentration can be found from the dose where the partial dose is defined by $\psi(x,y,z,t) = \int_0^t C(x,y,z,t')dt'$ and the total dose by $\psi_\infty = \psi(x,y,z,\infty)$. For clouds with short passage times over a receptor, the average concentration $\overline{C}$ can be obtained from $\overline{C} = (\psi(t_2) - \psi(t_1))/T_a$, where the averaging time $T_a = t_2 - t_1$. If the puff passage time $4\sigma_{rx}/U$ is less than T_a, then $\overline{C} = \psi_\infty/T_a$.

Cloud rise and inversion penetration. Scorer (1978) combined theory and laboratory experiments to obtain the following expression for cloud rise in a neutral environment

$$\Delta h = 2.35(M_T t + F_T t^2)^{1/4} . \quad (3)$$

M_T and F_T are the initial momentum and buoyancy of the cloud and are given by

$$M_T = \frac{4\pi}{3} r_o^3 w_o \quad \text{and} \quad F_T = \frac{gQ_T}{c_p \rho_a \Theta_a} , \quad (4)$$

where w_o, r_o, and Q_T are the initial velocity, radius, and heat content of the thermal, g is the gravitational acceleration, c_p is the specific heat of air, and ρ_a and Θ_a are the ambient air density and potential temperature.

Scorer also found the puff radius to be $r = \alpha\Delta h_t$, where Δh_t is the cloud top height and α is an empirical entrainment coefficient. α ranged from 0.14 to 0.5 with a mean of 0.25. The relative dispersion $\sigma_r = r/\sqrt{2}$.

Using field observations, Weil (1982) confirmed that Eq. (3) was a good fit to data over a wide range of times. Thus, Eq. (3) is suitable for the initial rise of a cloud, i.e., before it is limited by stable stratification. The Q_T can be determined from the mass of the detonation and its heat content, $H = 1100$ kcal/kg TNT equivalent.

For cloud penetration of an elevated density jump, results have been found from laboratory experiments in a nonturbulent environment. Richards (1961) obtained an empirical expression for the fraction P of the cloud penetrating the jump: $P \simeq 1 - 0.5\Delta\rho_i/\Delta\rho_{Ti}$, where $\Delta\rho_i$ is the density jump and $\Delta\rho_{Ti}$ is the average density excess of the cloud when it reaches the jump. The $\Delta\rho_{Ti}$ can be estimated from F_T and r.

The $\Delta\rho$ in a detonation cloud is related to the cloud temperature excess $\Delta\Theta$ by $\Delta\rho/\rho_a = \Delta\Theta/\Theta_a$ with $\Delta\Theta = (3/4\pi)Q_T/(\rho_a c_p r^3)$. We can then rewrite Richards' expression as $P = 1 - (2\pi/3)(\Delta\Theta_i \rho_a c_p \alpha^3 h^3/Q_T)$, where $\Delta\Theta_i$ is the temperature jump at $z = h$. The h_s is assumed to be zero so that the cloud radius at the inversion is αh. The above relationship shows the strong sensitivity of P to αh.

Figure 1 shows examples of P versus the detonation mass W, where we have used $Q_T = W \cdot H$ and $\alpha = 0.25$. For $h = 500$ m, one can see that a significant fraction of the cloud material penetrates the temperature jump for $\Delta\Theta_i = 1$ or 3°C. However, for $h = 1000$ m, the P is significantly reduced.

A more realistic temperature distribution above the CBL is a constant $\partial\Theta_a/\partial z$. Experiments simulating this distribution as well as a jump above a well-mixed layer are currently underway in a salt-stratified tank at the EPA Fluid Modeling Facility in North Carolina.

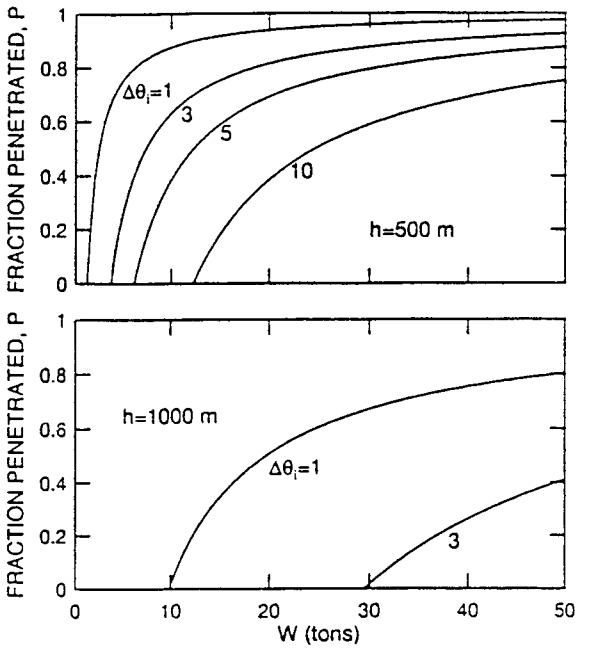

Fig. 1. Fraction of cloud penetrating an elevated temperature jump ($\Delta\Theta_i$, °C) as a function of detonation mass.

Dispersion parameters. For clouds, σ_r is dominated by entrainment for short times with $\sigma_r = \sigma_{rb} = 0.18\Delta h$. At intermediate times ($t < T_L$), the σ_r may be dominated by ambient turbulence in the inertial subrange with $\sigma_r \sim \sigma_{ra} = a_1\epsilon^{1/2}t^{3/2}$, where T_L is the Lagrangian time scale, ϵ is the turbulent kinetic energy dissipation rate, and a_1 is a constant (see Thomson, 1990). At long times ($t \gg T_L$), $\sigma_{ra} = (2\sigma_w^2 T_L t)^{1/2}$ for homogeneous isotropic turbulence. For σ_{ra}, we use an interpolation expression of the form $\sigma_{ra} = a_1\epsilon^{1/2}t^{3/2}/(1+a_2 t/T_L)$ to satisfy the intermediate- and long-time results. In addition, ϵ can be written as $\epsilon = b\sigma_w^2/T_L$ in homogeneous isotropic turbulence.

In a strong CBL, the following approximations can be made for $z \geq 0.1h$: $\epsilon \simeq 0.4w_*^3/h$, $\sigma_w \simeq 0.6w_*$, and $T_L \sim 0.7h/w_*$ (Weil, 1988). These approximations coupled with $\epsilon = b\sigma_w^2/T_L$ lead to $b = 0.78$. To satisfy the long-time σ_{ra} limit, we must have $a_2 = 0.62a_1$; a_1 is estimated to be 0.57 from Thomson's two-particle model results. The resulting parameterization for σ_{ra} in the CBL is

$$\frac{\sigma_{ra}}{h} = \frac{0.36X^{3/2}}{1+0.51X} \quad \text{with} \quad X = \frac{w_* x}{Uh}, \qquad (5)$$

where we have assumed $t = x/U$.

To connect the short-, intermediate-, and long-time relative dispersion regimes in a continuous manner, we adopt the following parameterization: $\sigma_r^3 = \sigma_{rb}^3 + \sigma_{ra}^3$. For clouds dominated by buoyancy, $\sigma_{rb} = 0.42F_T^{1/4}t^{1/2}$.

The total or absolute dispersion is necessary to estimate the C for a meandering puff or plume. The σ_x and σ_y in Eq. (2) can be obtained from a parameterization of Taylor's theory: $\sigma_x = \sigma_u t/(1+t/2T_{Lx})^{1/2}$ and similarly for σ_y. The T_{Lx} is the Lagrangian time scale for the u component and can be parameterized by $T_{Lx} \propto \sigma_u/h$, etc. (e.g., see Venkatram and Wyngaard, 1988). For the CBL and the results below, we use $T_{Lx} = T_{Ly} = 0.7h/w_*$ and $\sigma_u = \sigma_v = 0.6w_*$.

3.2 *Some Results*

We have computed the C_c in the buoyant puff and the mean GLC along $y = 0$ due to a meandering puff for $0.1 \leq W \leq 50$ tons. The σ_r, σ_x, and σ_y were calculated as described above. In the following, the cloud buoyancy is characterized by its dimensionless value

$$F_{T*} = \frac{F_T}{w_*^2 h^2}\ ; \qquad (6)$$

we used $w_* = 2$ m/s, $h = 1000$ m, and $U = 5$ m/s.

Figure 2 shows the dimensionless concentration $C_c h^3/Q$ as a function of X. We have neglected cloud penetration of the inversion but included cloud reflection at $z = 0, h$ and assumed that $h_e = \text{Min}(\Delta h, h)$. The large variation in the dimensionless C_c at short range ($X < 1$) is due to the buoyancy-induced dispersion σ_{rb}. As can be seen, $C_c h^3/Q$ decreases systematically and significantly with an increase in F_{T*} due to the increase in σ_{rb} with F_{T*}. For $X > 1$, the curves converge to the same limit because at long times the σ_r is dominated by σ_{ra}, which is independent of F_T.

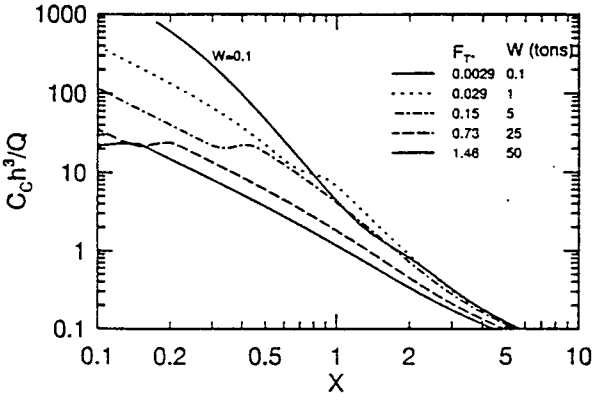

Fig. 2. Dimensionless concentration at cloud centroid versus dimensionless downwind distance.

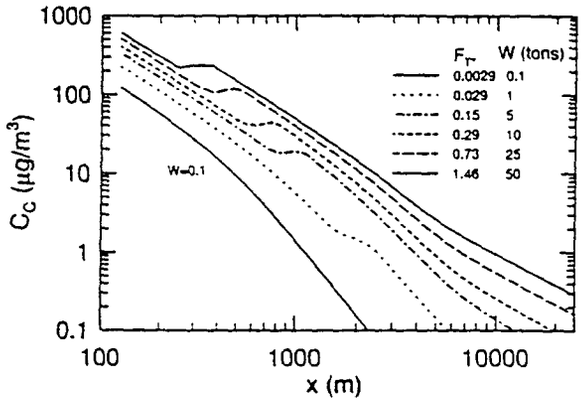

Fig. 3. SO_2 concentration at cloud centroid versus downwind distance.

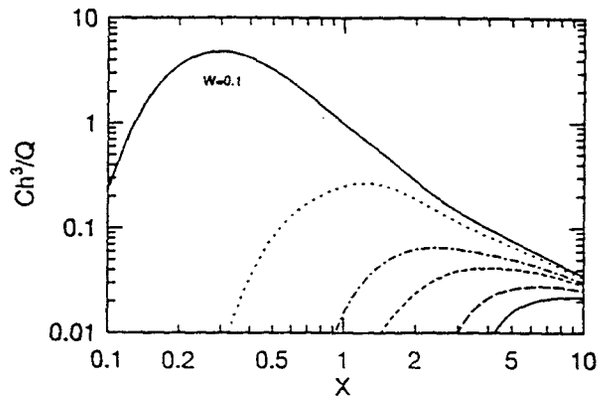

Fig. 4. Dimensionless mean ground-level concentration of cloud versus dimensionless downwind distance; see Fig. 3 for key to lines.

Figure 3 shows dimensional values of the peak (C_c) SO_2 concentrations in the cloud, with $Q = W \cdot E_f$ where E_f ($= 2.23 \times 10^{-4}$; Andrulis, 1992) is the SO_2 emission factor. In Fig. 3, the order of the curves is reversed from Fig. 1—the curve for $W = 50$ tons exhibits the highest C_c. The reversal is due to the increase in Q with W, which overcomes the decrease in C_c due to the increase in σ_{rb} with F_T. At small x, all of the curves have the same slope: $C_c \propto x^{-3/2}$ because $\sigma_{rb} \propto x^{1/2}$. Some curves exhibit a short region of a nearly constant C_c with x; this is due to puff trapping in the CBL. At large distances ($x > 10$ km), clouds for all cases become uniformly mixed in the vertical but continue to spread laterally; thus, $C_c \propto Q/\sigma_{ra}^2 \propto Q/x$ as shown.

The dimensionless mean GLC, Ch^3/Q, along the puff centerline is shown in Fig. 4; this mean is for an ensemble of meandering puffs and is obtained from Eq. (2) with reflection terms included. Again, the highest dimensionless concentration occurs for the smallest F_{T*}; this is attributed to the smaller Δh for the smaller detonations. Likewise, the increase in the distance to the maximum concentration with F_T is due to the increase in Δh. Note that for $X < 1$, the Ch^3/Q can be two orders of magnitude smaller than the $C_c h^3/Q$ (Fig. 2) at the same X value, but at $X \simeq 10$, the curves from both figures converge to the same limit. This occurs because the puff becomes uniformly mixed in z and the $\sigma_x, \sigma_y \simeq \sigma_{ra}$ at large t or x.

Figure 5 shows the mean dimensional GLC for the same range of W and F_T values as in Figs. 2 - 4. Several interesting features are found: 1) A non-monotonic variation occurs in the maximum GLC C_m with W and F_T. 2) The variation in C_m for $0.1 \leq W \leq 50$ tons is only about a factor of 4 even though the range in Q is a factor of 500; the weak dependence on Q is attributed to the increase in Δh with F_T. 3) The C_m is of the order of 0.1 μg/m³, which is the lower bound for C_c in Fig. 3.

We should clarify again the meaning and use of C in Figs. 4 and 5. It is the mean GLC along $y = 0$ due to an ensemble of meandering puffs and probably has little to do with an observed centerline GLC in an individual puff. This computed C is to be used together with a modeled σ_c in a concentration probability distribution to estimate the peak short-term GLC that could occur downstream of the detonation. The peak GLC would correspond to some specified probability level.

4. SHORT-DURATION RELEASES

4.1 *Dispersion Model*

For short-duration releases or burns, our general approach is an integrated puff model in which the short-term mean concentration relative to the puff centerline is

$$C = \int_0^{t_r} \frac{Q_r \, f(t') \, dt'}{(2\pi)^{3/2} \sigma_{rx} \sigma_{ry} \sigma_{rz}} \qquad (7a)$$

$$f = \exp\left[-\frac{(x - U(t - t'))^2}{2\sigma_{rx}^2} - \frac{y^2}{2\sigma_{ry}^2} - \frac{z'^2}{2\sigma_{rz}^2} \right], \qquad (7b)$$

where t' is the puff emission time, t_r is the total release duration, Q_r is the continuous source emission rate, $z' = z - h_e$, $\sigma_{rx} = \sigma_{rx}(t - t')$, and similarly for σ_{ry}, σ_{rz}. The integration in (7a) can be carried out analytically for limiting forms of $\sigma_{rx}(t - t')$, etc., but must be done numerically

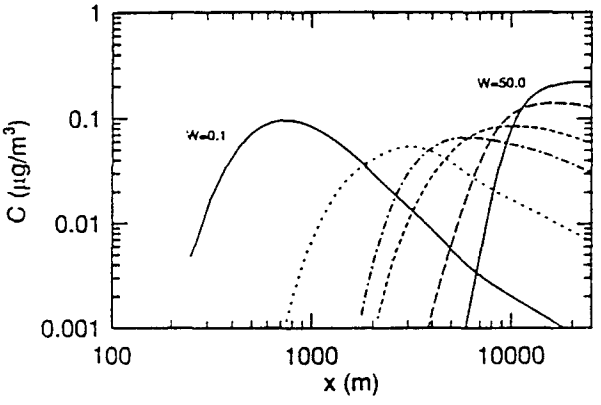

Fig. 5. Mean ground-level SO_2 concentration of cloud versus downwind distance; see Fig. 3 for key to lines.

in general. Numerical integration is required when using the parameterization $\sigma_{rx} = \sigma_{ry} = \sigma_{rz} = \sigma_r = a_1\epsilon^{1/2}(t-t')^{3/2}/(1+a_2(t-t')/T_L)$.

The integrated puff model also can be used for the mean concentration of meandering puffs by replacing the relative dispersion by the absolute dispersion.

In the following, we focus on the C_c for a short-duration release (burn) and consider two limiting cases. 1) For $t < t_r$, we expect the rise and dispersion of the integrated puff to reduce to that of a continuous plume for sufficiently strong winds such that the relative dispersion in the x direction can be neglected. 2) For $t > t_r$, the C field should reduce to that for an instantaneous puff but with $Q = Q_r t_r$ and $F_T = (4\pi/3)F_b t_r$, where F_b $(= w_o r_o^2 g \Delta\Theta_o/\Theta)$ is the continuous source buoyancy flux. As will be shown below, the C_c for the long-time puff solution is lower than that for the plume solution. Thus, we take the plume solution as an upper bound and $C_c = \mathrm{Min}(C_{cpl}, C_{cpu})$, where C_{cpl} and C_{cpu} denote the C_c values for the plume and puff, respectively.

The mean concentration field relative to the plume centerline is given by

$$C = \frac{Q_r}{2\pi U \sigma_{ry}\sigma_{rz}} \exp\left(-\frac{y^2}{2\sigma_{ry}^2} - \frac{(z-h_e)^2}{2\sigma_{rz}^2}\right) . \quad (8)$$

Here, the plume rise is attributed to buoyancy and is given by $\Delta h = 1.6F_b^{1/3}x^{2/3}/U$ and its radius is $r = 0.4\Delta h$ (Briggs, 1984). Source momentum effects can be included in the future. As with the puff model, we will assume $\sigma_{ry} = \sigma_{rz} = \sigma_r$ and $\sigma_r^3 = \sigma_{rb}^3 + \sigma_{ra}^3$. The σ_{ra} is given by Eq. (5) and the plume $\sigma_{rb} = r/\sqrt{2} = 0.45F_b^{1/3}x^{2/3}/U$. The $C_c = Q_r/(2\pi U\sigma_r^2)$ from Eq. (8); these expressions can be expanded to include reflection at $z = 0, h$.

To demonstrate the applicability of the instantaneous puff model (Eq. 1) for long times—$t > t_r$ and $t > T_L$, we carry out the integration in Eq. (7a) for $\sigma_{rx} = \sigma_{ry} = \sigma_{rz} = \sigma_r = (2\sigma_w^2 T_L t)^{1/2}$ and assume $\sigma_u = \sigma_v = \sigma_w$. We ignore the dependence of Δh on t'. The result is

$$C = \frac{Q_r}{4\pi\sigma_r^2}\exp\left(\frac{U}{2\sigma_w^2 T_L}(x-r)\right) \times$$

$$\left[\mathrm{erf}\left(\frac{r-U(t-t_r)}{\sqrt{2}\sigma_r}\right) - \mathrm{erf}\left(\frac{r-Ut}{\sqrt{2}\sigma_r}\right)\right] , \quad (9)$$

where erf is the error function and $r^2 = x^2 + y^2 + (z-h_e)^2$. We evaluate this expression at a t corresponding to the center of the cloud, $x = U(t - t_r/2)$, or $t = x/U + t_r/2$. The C_c is found to be $C_c = Q_r t_r/[(2\pi)^{3/2}\sigma_r^3]$. This result supports the use of the instantaneous puff model, with $Q = Q_r t_r$, for the long-time limit of a finite-duration release.

4.2 *Some Results*

Results are presented for the dimensionless concentration $C_c U h^2/Q_r$ for the plume and instantaneous puff models, with reflection at $z = 0, h$ included in both. The continuous source buoyancy flux is characterized by its dimensionless value:

$$F_* = \frac{F_b}{U w_*^2 h} . \quad (10)$$

Figure 6 shows the dimensionless C_c for the plume model with F_* in the range $0.001 \le F_* \le 0.3$. The trends appear similar to those for the puff model in Fig. 2 although the variation of $C_c U h^2/Q_r$ with F_* is not as great as for the puff model. For $X < 1$, the decrease in the dimensionless C_c with increasing F_* is due to the increase in σ_{rb} with F_b. For $X > 1$, all of the curves approach the same asymptotic curve; this is due to the dominance of σ_{ra} at large times and its independence of F_b.

Figure 7 presents the dimensionless C_c for both the plume and puff models for $F_* = 0.001$ and 0.01 and various values of $t_{r*} = t_r w_*/h$. The time scale $h/w_* = 500$ s for the w_* (= 2 m/s) and h (= 1000 m) used here, so that t_r ranges from 50 s to 500 s or about 1 to 8 min. The plume C_c is chosen as long as it exceeds the puff C_c. As can be seen, the distance over which the plume solution applies increases as t_{r*} does.

5. ACKNOWLEDGMENTS

This work has been supported by the DOD/DOE Strategic Environmental Research and Development Program. We are grateful to Seth White for producing the figures.

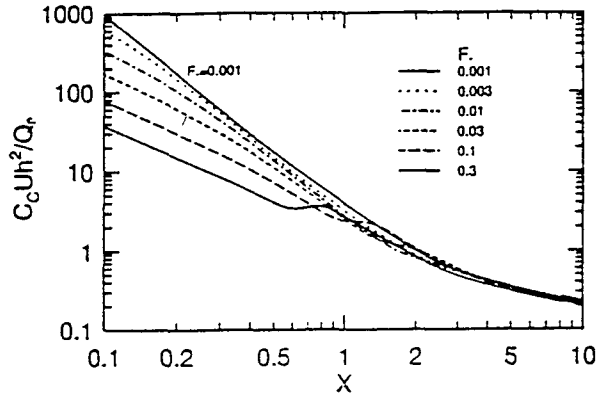

Fig. 6. Dimensionless concentration at plume centroid versus dimensionless downwind distance.

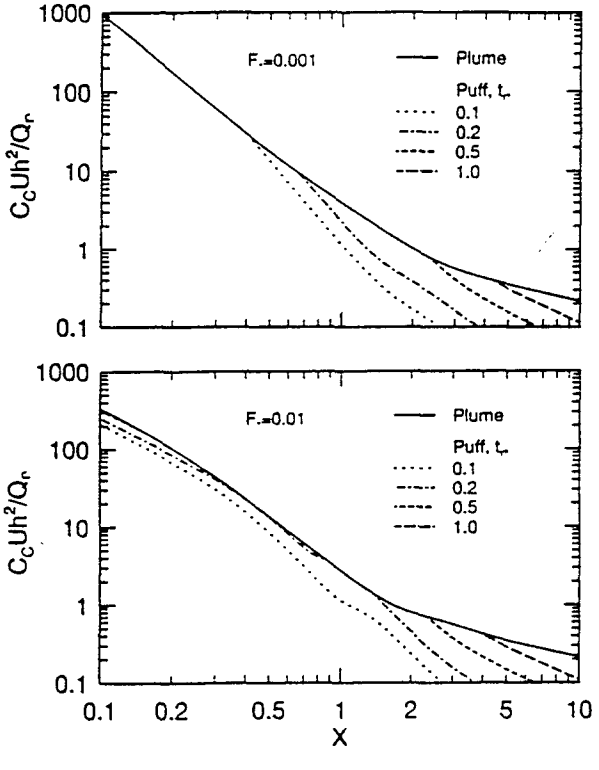

Fig. 7. Dimensionless concentration at plume and puff centroid versus dimensionless downwind distance.

6. REFERENCES

Andrulis Research Corporation, 1992: Development of methodology and technology for identifying and quantifying products from open burning and open detonation thermal treatment methods. Bangbox test series, Vol. 1, Final Rpt., US Army, Rock Island, IL.

Briggs, G.A., 1971: Some recent analyses of plume rise observations. In: *Proceedings of the Second International Clean Air Congress*, H.M. Englund and W.T. Beery, Eds., Academic Press, NY, 1029–1032.

Briggs, G.A., 1984: Plume rise and buoyancy effects. *Atmospheric Science and Power Production*, D. Randerson, Ed., US Dept. of Energy DOE/TIC-27601, 327–366.

Deardorff, J.W., and G.E. Willis, 1988: Concentration fluctuations within a laboratory convectively mixed layer. *Lectures on Air Pollution Modeling*, A. Venkatram and J.C. Wyngaard, Eds., Amer. Meteor. Soc., Boston, 357–384.

Irwin, J.S., 1983: Estimating plume dispersion—A comparison of several sigma schemes. *J. Climate Appl. Meteor.*, **22**, 92–114.

Petersen, W.B., 1986: A demonstration of INPUFF with the MATS data base. *Atmos. Environ.*, **20**, 1341–1348.

Richards, J.R., 1961: Experiments on the penetration of an interface by buoyant thermals. *J. Fluid Mech.*, **11**, 369–384.

Scorer, R.S., 1978: *Environmental Aerodynamics*, Halsted Press, New York.

Thomson, D.J., 1990: A stochastic model for the motion of particle pairs in isotropic high-Reynolds-number turbulence, and its application to the problem of concentration variance. *J. Fluid Mech.*, **210**, 113–153.

Venkatram, A., and J.C. Wyngaard, Eds., 1988: *Lectures on Air Pollution Modeling*, Amer. Meteor. Soc., Boston, 390 p.

Weil, J.C., 1982: Source buoyancy effects in boundary layer diffusion. *Workshop on the Parameterization of Mixed Layer Diffusion*, Physical Sciences Laboratory, New Mexico State Univ., Las Cruces, 235–246.

Weil, J.C., 1988: Dispersion in the convective boundary layer. *Lectures on Air Pollution Modeling*, A. Venkatram and J.C. Wyngaard, Eds., Amer. Meteor. Soc., Boston, 167–227.

Weil, J.C., B. Templeman, R. Banta, and W. Mitchell, 1995: Atmospheric dispersion model development for open burn/open detonation emissions. Paper no. 95-MP22A.05 presented at 88th Annual Meeting of the Air and Waste Management Association, AWMA, Pittsburgh, PA.

Wyngaard, J.C., 1988: *Lectures on Air Pollution Modeling*, A. Venkatram and J.C. Wyngaard, Eds., Amer. Meteor. Soc., Boston, 9–61.